



SEISMIC FRAGILITY FUNCTIONS OF METRO TUNNELS

G. Candia⁽¹⁾, B. Lyon⁽²⁾, J. Macedo⁽³⁾, R. Cornejo⁽⁴⁾

⁽¹⁾ Associate Professor, Faculty of Civil Engineering at Universidad del Desarrollo, Chile. National Research Center for Integrated Natural Disaster Management CONICYT/FONDAP/15110017, gcandia@udd.cl

⁽²⁾ Master of Science, Faculty of Civil Engineering at Universidad del Desarrollo, Chile, b.lyon@udd.cl

⁽³⁾ Assistant Professor, Georgia Institute of Technology, United States, jorge.macedo@gatech.edu

⁽⁴⁾ Graduate student, Georgia Institute of Technology, United States, rcornejot@uni.pe

Abstract

The seismic response of metro tunnels is of major importance for the sustainability of urban centers, as tunnels are critical elements of metro networks and they transport millions of passengers per day. Although ground tunnels may suffer less damage than conventional aboveground structures, recent experimental and post-earthquakes reconnaissance studies have shown that extensive damage under typical design earthquake scenarios may be possible. Evaluating the seismic response of metro tunnels on a scenario-based approach is difficult without a well-calibrated numerical constitutive model suitable for soil-structure interaction problems. In addition, published fragility functions for tunnels are very scarce; most of them developed for tunnels in regions affected by shallow crustal earthquakes, and derived from numerical analyses that rely on a small number of ground motions recordings. Traditional approaches may provide reasonable estimates of the median tunnel response; however, they are not well suited to characterize the uncertainty in the response, which is vital for risk-based assessments. To address some of these limitations, the current study uses a performance-based approach to estimate mean rates of exceedance of critical engineering demand parameters (EDPs) used in tunnel design (e.g., internal forces on the lining, diametral strains, ground deformation parameters, among others). Additionally, a new set of fragility functions for EDPs are developed taking into account an earthquake dataset with large number of records to capture the mean EDP values as well as a quantification of uncertainties. The fragility functions are derived from finite element model (2D) and dynamic analyses of a dual-track circular tunnel on medium dense soil; the tunnel has a depth of 15 m, 6 m in diameter, and a 30 cm thick sprayed concrete lining with steel rebar, a typical design for interstation tunnels used in dense urban areas. The numerical model implemented in OpenSees uses linear elastic elements for the lining and the non-linear pressure dependent constitutive model PDMY02 [1] to model the soil response. To guarantee reliable simulations, the model parameters were validated with dynamic centrifuge test results of a circular tunnel on Leighton Buzzard Sand (LBS) subjected to harmonic base excitation, laboratory tests for the sand, and results derived from the theory of elasticity. The numerical model considers a no-slip condition for the soil-structure interaction. The numerical model captured the stiffness, strength, and energy dissipation properties of the materials, as well as the dynamic response of the soil deposit and the tunnel. The preliminary results show that the peak ground acceleration at bedrock is an efficient intensity measure to characterize the tunnel response at shallow crustal regions.

Keywords: tunnels, seismic fragility functions, performance-based design, numerical modelling, damage parameters

1. Introduction

Urban tunnels are a critical component of transport infrastructure; in seismic regions, these systems must remain operational and not suffer damage after an exceptionally severe earthquake. Although tunnels are regarded as seismically safe structures, there is a possibility that a tunnel will experience significant damage during its lifespan, which can lead to cascading effects of direct and indirect consequences. For example, the Metro system in Santiago, Chile, has a tunnel network of more than 140 km and transports almost 2.6 million passengers daily. A severely damaged arc of the network can lead to loss of human lives, extended service interruptions (e.g., weeks or months), and economic losses to the state.



Recent histories show that tunnels can suffer significant damage due to high ground shaking levels and site amplification effects, which increase the level of deformations in the tunnel [2]. For instance, Power et al. [3] analyzed more than 200 cases of seismic tunnel response, mostly from the 1995 Kobe earthquake (Mw 7.5) and the 1994 Northridge earthquake (Mw 6.7). The authors conclude that underground structures are less vulnerable to earthquake damage relative to ordinary aboveground structures (i.e., fixed base, without added energy dissipation), and that tunnels through soil exhibit higher damage rates than rock tunnels. Most importantly, tunnels that suffered severe damage or collapse typically involve some form of ground failure (e.g., liquefaction, slope failures in tunnel portals, or tunnels across active faults, among others). Likewise, Yashiro et al. [4] documented the tunnels damaged during the 1923 (Mw 7.9) Kanto earthquake in Japan, where over 90 tunnels near the rupture area were damaged and service was interrupted for approximately 2 months. The study also documents the response of tunnels during the 2004 Niigataken-Chuetsu earthquake (Mw 6.8), where 24 tunnels were damaged. During the 1989 Loma Prieta earthquake (Mw 6.9) no damage was reported on the BART (Bay Area Rapid Transit) tunnels in San Francisco and the Los Angeles Metro [5]; indeed, these systems were operative within 24 hours of the earthquake. In contrast, the Oakland-Alameda tube suffered extensive cracking due to lining deformations induced by liquefaction of the surrounding media.

Kuesel [6] developed a simplified soil structure interaction (SSI) method to evaluate the seismic response of tunnels, which was then applied in the design of BART. His pioneering work led to further developments of 'deformation analyses', in which the ground deformations due seismic waves are transmitted to the lining. The author noted that small diameter tunnels (e.g., buried pipelines, conduits), are more sensitive to tensile deformations and shear deformations occurring along the tunnel's axis, whereas larger tunnels (e.g., metro systems) are more sensitive to shear deformations parallel to the tunnel's cross section.

Estimating the seismic tunnel deformation and internal forces remains a challenging problem in earthquake engineering. Available methods range from simplified analytical solutions based on the theory of elasticity (e.g., [7, 8]), sophisticated numerical analyses (e.g., [2]), and experimental methods [9-11], out of which the geotechnical centrifuge is one of the most reliable for studying scaled models. Its main advantage over 1-g shaking tables is the ability to simulate dynamic stress increments; on the other hand, centrifuge models do not reproduce K_0 conditions very accurately, which could be a limitation in many practical cases. Recently, Lanzano et al. [12] studied the seismic response of tunnels in dry sand in the centrifuge at Schofield Centre, UK. The main objective of this experiment was to characterize the dynamic SSI and obtain benchmark response histories to calibrate numerical models. Contrary to the low risk perception that many engineers have on tunnels, this study concludes that tunnels may undergo significant damage during strong seismic events. After the work by [12], five research teams performed a numerical round-robin to simulate the centrifuge models using state-of-the-art software. All participants were given the same information to build their numerical models (e.g., soil parameters, geometry, base excitation) and performed blind prediction of the key response parameters, including ground acceleration, tunnel deformations and internal forces. The five groups matched the ground acceleration histories at several locations reasonably well. However, the bending moments in the tunnel could not be reproduced numerically.

Despite the recent advances in the characterization of seismic tunnels response, computing risk in these complex SSI systems is not straightforward. Available fragility functions for deep rock tunnels (e.g., [13]) or tunnels through alluvial deposits (e.g., [14]) have been derived from a small number of ground motions, and therefore, more research is required to characterize the propagation of ground motion uncertainties and the influence of different ground motion datasets on the tunnel response. The present work develops vulnerability functions for a circular tunnel in medium dense sand using a performance based approach. The results are derived from a finite element implementation of a soil-tunnel system subjected to 285 ground motions from shallow crustal earthquakes, allowing for a hazard-consistent assessment of risk variables.



2. Numerical Modeling

Fragility functions for key response parameters of a circular tunnel in dry Leighton Buzzard Sand (LBS) [15] were obtained from a plain strain finite element model implemented in OpenSees [16]. The model geometry is based on the scaled centrifuge test by Lanzano et al. [12], which consist of a 23.2 m × 40 m (height × width) soil deposit and a circular tunnel 6 m in diameter located 12 m below the surface. The model geometry was discretized in 1328 nodes, 1238 quadrilateral soil elements, and 40 linear-elastic frame elements in no-slip conditions to represent the sprayed-concrete lining as shown in Fig.1(a). The stress-strain relation of LBS elements is described using the PressureDependMultiyield constitutive PDMY02 [1], with model parameters characteristic of a medium dense sand ($D_r = 75\%$, $G_s = 2.65$, $e_{min} = 0.613$ y $e_{max} = 1.014$). The small strain shear modulus (also referred to as G_{max}) was defined as $G/p_a = G_b f_1(e) f_2(p')$ [17], with $G_b = 1155$, $f_1(e) = (2.17 - e)^2 / (1 + e)$ and $f_2(p') = (p'/p_a)^{0.5}$, where $p_a = 100$ kPa. Profiles of G/p_a versus depth are presented in Fig.1(b) and the parameters of the PDMY02 model are shown in the Table 1.

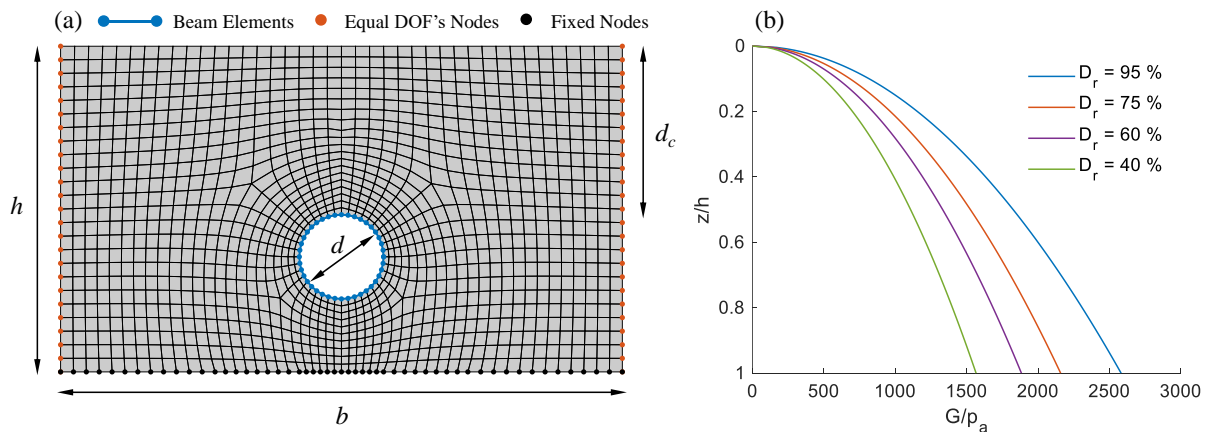


Fig. 1 – (a) Finite element mesh of the soil-tunnel system ($h = 23.2$ m, $b = 40$ m, $d_c = 12$ m, $d = 6$ m), and (b) depth profiles of shear modulus for different relative densities

Table 1 – Model parameters for LBS using the constitutive relation PDMY02

Density	ρ	=	1.55	ton/m ³
Reference shear modulus	G_r	=	143	MPa
Reference bulk modulus	B_r	=	310	MPa
Friction angle	ϕ_c	=	32	deg
Peak shear strain	γ_{max}	=	0.1	
Reference confining pressure	p_r'	=	100	kPa
Pressure dependent coefficient	d	=	0.5	
Phase transformation angle	ϕ_{PT}	=	27	deg
Contraction	ct	=	0.05	
Dilation 1	di_1	=	0.6	
Dilation 3	di_3	=	3	
Initial void ratio	e	=	0.71	

To create the soil mesh we adopted the recommendations by Kuhlemeyer & Lysmer [18], who prescribe elements of maximum size $\Delta l = V_s / (8f_{max})$, where $V_s = 300$ m/s is the average shear wave velocity of the soil and f_{max} the maximum frequency of interest. Both, the centrifuge ground motions and the ground motion dataset used to compute risk (discussed in the next section) deliver most of the energy in frequencies up to 30-35 Hz, which results in $\Delta l = 1$ m. To simulate the free field boundary conditions of the centrifuge experiment, an ‘equalDOF’ constraint was assigned to the edge nodes, such that pairs of nodes having the same elevation share the same horizontal displacements and vertical displacements. In addition, the base



nodes were fixed in both directions. To compute fragility functions and risk, we adopted a three-step procedure: (i) estimation of seismic hazard at the tunnel site and ground motion selection, (ii) for each selected ground motion, computation of the tunnel response parameters from a non-linear dynamic analysis, and (iii) computation of the mean annual rate of exceedance of the tunnel response parameters.

In the current study, we analyze a hypothetical tunnel located in Oakland-CA and selected 285 shallow crustal ground motions from the PEER NGA database. The scaling of ground motions, required to simulate severe earthquake loading, was performed with the Conditional Scenario Spectra (CSS) method [19]; this method assigns each ground motion in the subset an annual rate of occurrence, such that the annual rate of exceedance of PGA and spectral ordinates is consistent with the seismic hazard obtained from standard seismic hazard calculations. The 5 % damped pseudo acceleration spectra of selected ground motions is shown in Fig.2(a), this particular subset allows to capture both the mean ground motion intensities and the uncertainty about the mean. The seismic hazard curves for PGA, and pseudo accelerations at periods $T = 0.3$ s and $T = 2.0$ s are presented in Fig.2(b), where dashed lines represent the hazard curves obtained from the 2014 National Seismic Hazard Map [20].

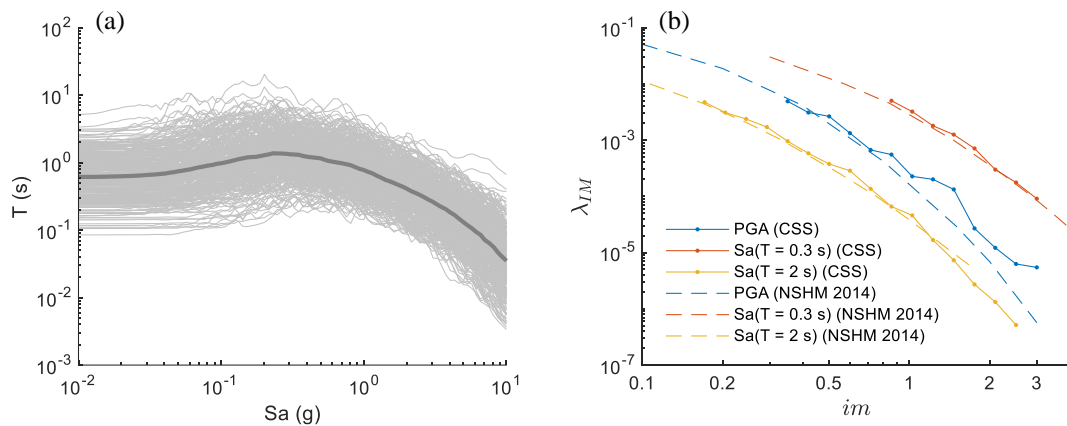


Fig. 2 – (a) Response spectra ($\xi = 5\%$) of selected ground motions and mean response spectrum; and (b) seismic hazard curves for Oakland, CA

The continuous dotted lines in Fig.2(b) represent the hazard curves reconstructed from the ground motion subset in accordance with Eq. (1), where $N_e = 285$ is the number of acceleration records, IM is the ground motion intensity (e.g., PGA or Sa ordinates), $rate_i$ is the occurrence rate assigned to the i -th ground motion, and H is the Heaviside function. The main advantage of the CSS approach for ground motion selection and scaling is that the rates of exceedance of tunnel response parameters are compatible with the seismic hazard.

$$\lambda_{IM} = \sum_{i=1}^{N_e} rate_i \cdot H(IM - im) \quad (1)$$

The equations of motion for the soil-tunnel system were solved using a Newmark scheme ($\gamma = 0.5$ y $\beta = 0.25$) and a uniform timestep $\Delta t = 0.001$ s. This scheme proved stable and simulations converged for all the 285 ground motions. In addition to the energy dissipated by hysteretic cycles, a minimum Rayleigh damping of $\xi_{\min} = 2\%$ at the fundamental frequency of the soil deposit $f_{\min} = 3.2$ Hz was supplemented for numerical stability and to attenuate high spurious frequencies.



3. Model Validation

The numerical model was validated at the element level through single element tests in cyclic simple shear, and at the free field level through the wave propagation on 1-D soil columns, where the ability to reproduce equivalent linear results was tested. Finally, the full model response was validated against the centrifuge test results by Lanzano et al. [12] using harmonic base excitations. No field data of actual tunnels during earthquakes is yet available for validating the finite element model at the required level of detail; thus, the current three-stage validation is our best estimate of the model parameters and will be used to compute tunnel responses due to severe ground motions.

A summary of the single element test results is presented in Fig.3, showing the shear modulus reduction curves and damping ratios versus shear strain. Notice that the PDMY02 curves are in good agreement with the empirical results by Seed and Idriss [21] and Darandeli [22] for medium dense sands, and the resonant column test conducted on LBS [23].

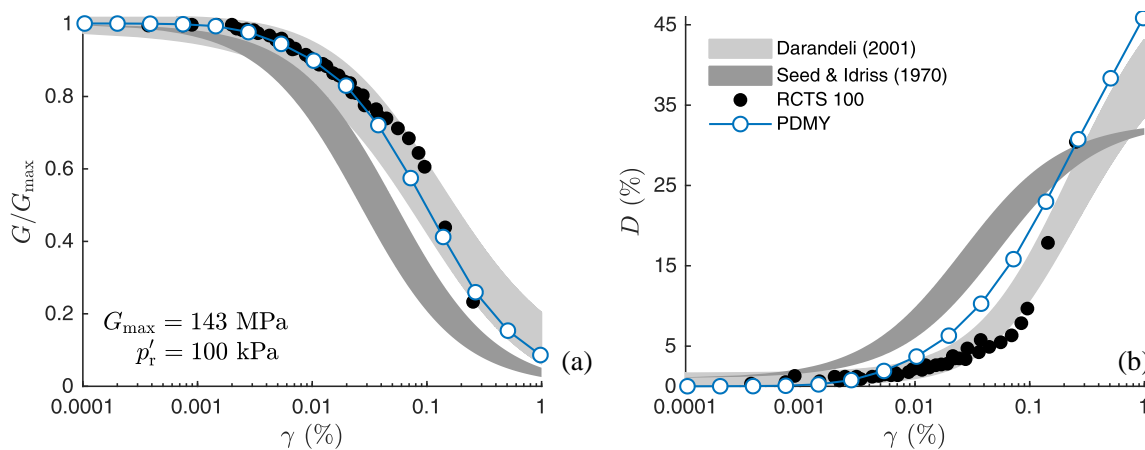


Fig. 3 – (a) Shear modulus reduction curves, and (b) damping amplification curves

The free field validation test results are presented in Fig.4. In this exercise, a 1-D soil column of PDMY02 elements was subjected to the Kobe (RSN1104) ground motion scaled to $PGA = 0.11$ g and $PGA = 0.05$ g. These two ground motion levels induce moderate to light stress non-linearity, with G/G_{max} values that drop as low as 68 % and 80 % at the bottom of the soil deposit, respectively. For both shaking intensities, the OpenSees implementation reproduces the surface response predicted by a linear equivalent SHAKE model in terms of acceleration time histories (not shown), peak ground acceleration (PGA), and pseudo accelerations. Thus, it is verified that the finite element model captures the soil stiffness and energy dissipation correctly.

In the final validation stage, the dynamic response of the soil-tunnel system was compared to Lanzano's [12] centrifuge experimental data. Four harmonic ground motions of increasing predominant frequency (0.375, 0.50, 0.625, 0.75 Hz) and increasing amplitude (0.05, 0.10, 0.12, 0.15 g, respectively) were used for comparison purposes. The acceleration histories computed in OpenSees are in excellent agreement with the measured response at multiple control stations, including points within the soil near to and away from the tunnel, as well as points located at the free surface. A comparison of acceleration time histories and 5% damped response spectra due to the 0.15 g amplitude motion is shown in Fig.5. Although some minor discrepancies are apparent at point A4 (located right underneath the tunnel), the computed response at points A6 and A8 (located right above the tunnel and at the free surface, respectively) matches the experimental data reasonably well, both in terms of amplitude and frequency content. In terms of volumetric response, the measured surface settlement at 10 m from the centerline was 7.8 cm, whereas the computed settlement was 6 cm. The remaining three ground motions led to good comparisons as well.

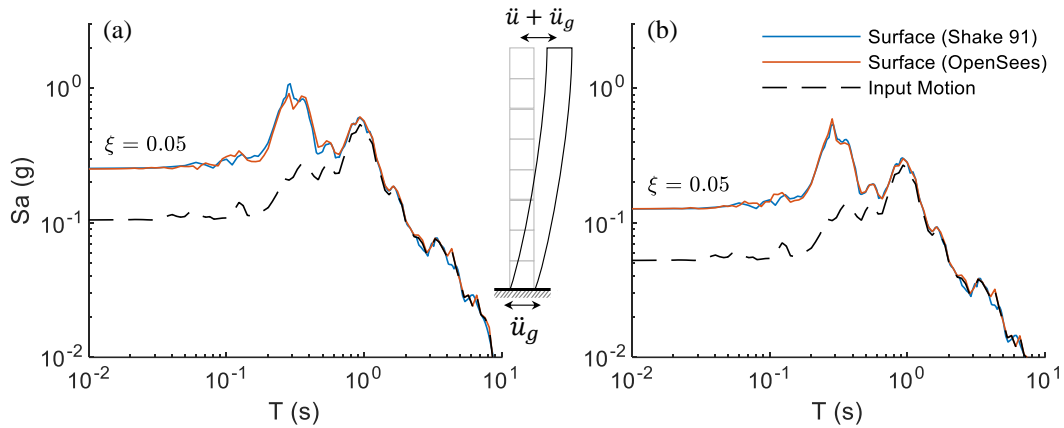


Fig. 4 – Comparison of 5 % damped response spectra on a 1-D soil column due to the Kobe (RSN1104) ground motion scaled to (a) PGA = 0.11 g, and (b) PGA = 0.05 g

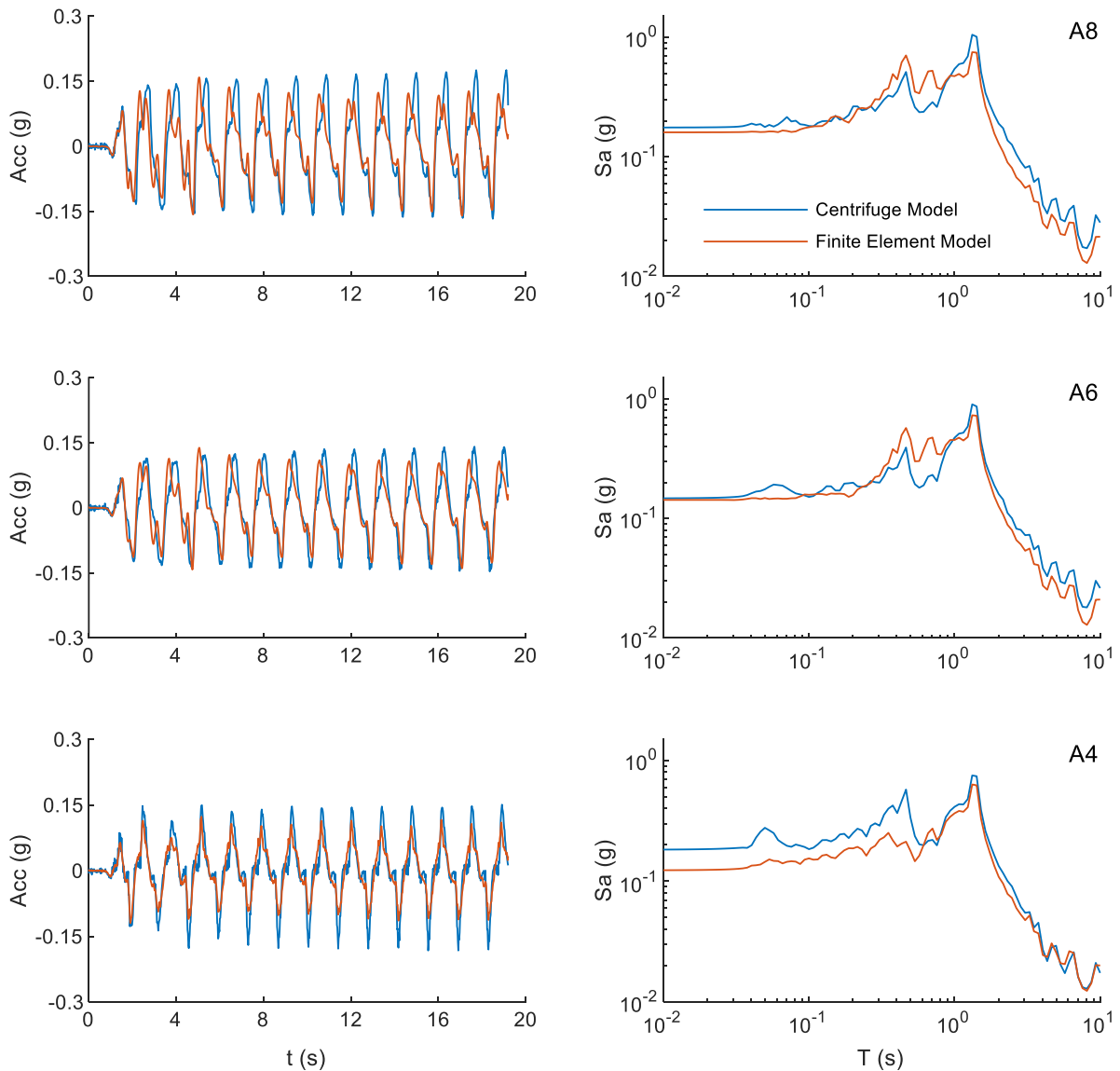


Fig. 5 – Comparison of acceleration histories (left plots) and response spectra (right plots) at three control points on a full 2D model. Harmonic input motion with predominant frequency 0.75 Hz and PGA = 0.15 g



4. Seismic Response

The finite element model was subjected to the 285 selected ground motions. Several model parameters were monitored and were later used to compute engineering demand parameters (EDPs), including the internal forces on the lining, the drift or ‘ovaling’ deformations, diametral strains, ground accelerations, among other. Because of the limitations of plain strain models to account for the construction sequence and stress buildup in the elements, EDPs such as forces or deformations are reported as increments relative to the initial static conditions, which in this case (e.g., medium dense sand) should not be a serious limitations. All the computations were performed in an Ubuntu Server 16.04.4 (128 GB RAM, 2 Intel Xeon processors E5-2660 v4 2.0GHz each) with a total runtime of approximately 14 days.

4.1 Internal lining forces

Fig.6 shows the largest curvature increment on the lining (moment increment normalized by the bending stiffness EI) as a function of three alternative intensity measures: peak ground acceleration PGA, peak ground velocity PGV, and the pseudo acceleration at the natural period of the soil deposit $Sa(T_0)$, with $T_0 = 0.3$ s, all three referred to the ground motion input (rock motion). From this figure, it is apparent that the median curvature increases linearly with the ground motion intensity in a log-log space, and that the uncertainty about the median remains approximately constant. A similar pattern was observed for axial forces and shear forces.

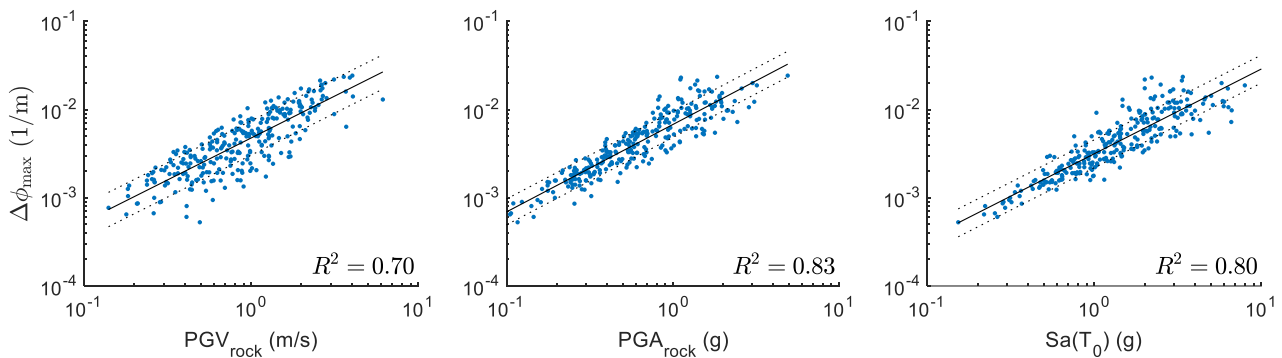


Fig. 6 – Dynamic increment of curvature as a function of PGV, PGA and $Sa(T_0)$

This result allows defining a linear scaling model for the internal forces as in Eq. (2), where ‘a’ and ‘b’ are regression parameters. Although there is no consensus among engineering on what is the most optimal or efficient ground motion intensity to characterize the seismic response of shallow tunnels (e.g., see discussion in [24]), the current study shows that PGA gives the largest coefficient of determination (R^2) in the linear regression out of the three IMs considered. Additionally, a normality tests was applied to the residuals and it is verified that they come from a normal distribution.

$$\ln \overline{EDP} = a \ln im + b \quad (2)$$

In addition, the axial load and bending moments on the lining were compared to the analytical solutions by Wang [7] and Penzien [8], who develop closed form equations for a tunnel on a linear elastic soil in no-slip conditions (i.e., no relative displacement between the soil and tunnel). The comparison was performed using the Kobe (RSN1113) ground motion scaled to PGA values of 0.12, 0.42 and 0.57g. The results in Fig.7 show that the computed bending moment distribution in the lining is consistent with Penzien’s [8] solution for the different intensity levels. On the other hand, the axial load falls in between Wang’s and Penzien’s solution for low shaking levels and approaches Penzien’s solution for high shaking levels. Similar results were observed for other ground motions; for more details, refer to [25].

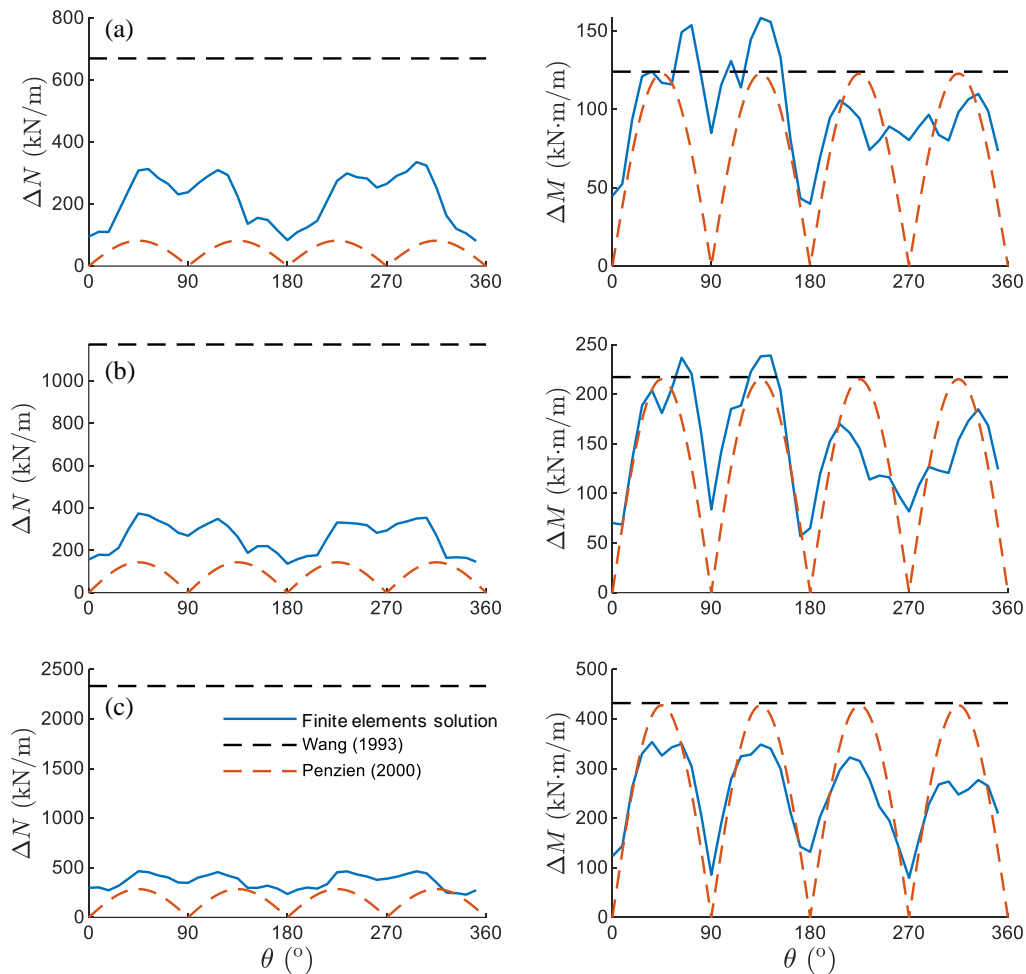


Fig. 7 – Dynamic increment of axial load (left) and bending moment (right) in the tunnel lining; comparison between finite element models and analytical solutions by Wang [7] and Penzien [8] for the ground motion Kobe (RSN1113) scaled to (a) PGA = 0.12 g, (b) 0.42 g, and (c) 0.57 g

4.2 Seismic Response of the soil and tunnel

The site amplification (bend over curves) at the free surface are shown in Fig.8 for point C, located above the tunnel, and point E located 20 m to the right. From these plots, it is apparent that input acceleration at bedrock are amplified up to $PGA_{rock} \approx 0.7$ g and are attenuated for larger PGA_{rock} values. The response of this soil deposit for $PGA_{rock} < 0.7$ g is similar to that of soil class AB and C3 according the Seed et al. [25].

Interestingly, the tunnel's drift ratio increases linearly with the average shear strain in the soil computed at a depth of 15 m away from the tunnel (point E). The direct implication is that the lining deformation of flexible tunnels (e.g., coefficient of flexibility $F = 18.3$ in this example) can be well approximated by the free field deformation [7], which greatly simplifies the analysis. Earthquake induced surface settlements up to 10 cm were computed in the simulations, which are the result of shear induced volumetric deformations. However, several ground motions with $PGA > 1$ g resulted in surface heaving; a close inspection of the data shows that the dilative response of the soil is caused by strong acceleration pulses at the early stages of ground shaking. Although this behavior is possible, the available experimental data is insufficient to validate this numerical result.

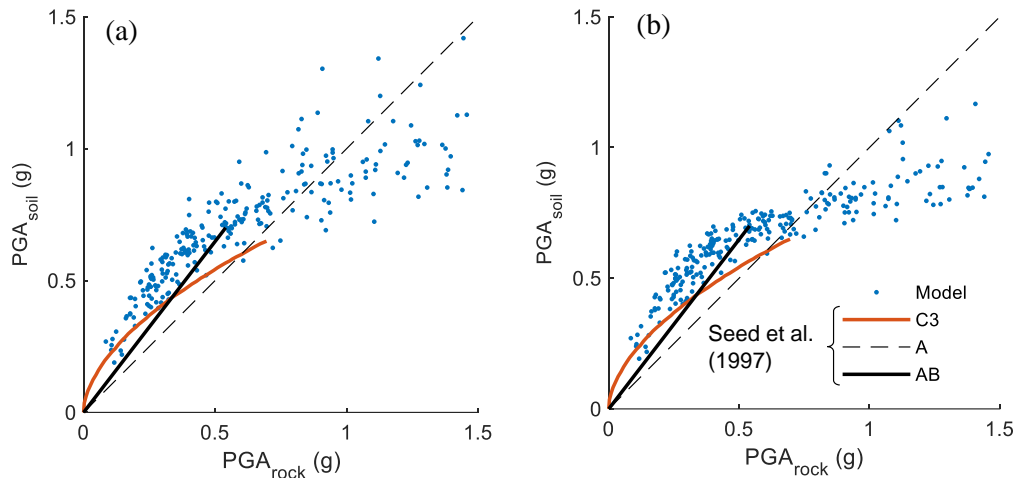


Fig. 8 – PGA amplification at the free surface at two locations: (a) above the tunnel, and (b) 10 m to the right of the tunnel

The tunnel distortion or ovaling can be described through the peak diametral strain, ε_{dmax} . Notice from the results in Fig.9 that ε_{dmax} takes mostly negative values (diameter contraction), but in cases of severe loading (e.g., $PGA > 1$ g) ε_{dmax} can also be positive. In any case, the peak distortions concentrate near the $\pm 45^\circ$ lines with respect to the horizontal, a result that is consistent with the observations by Penzien [8] and Anderson [26].

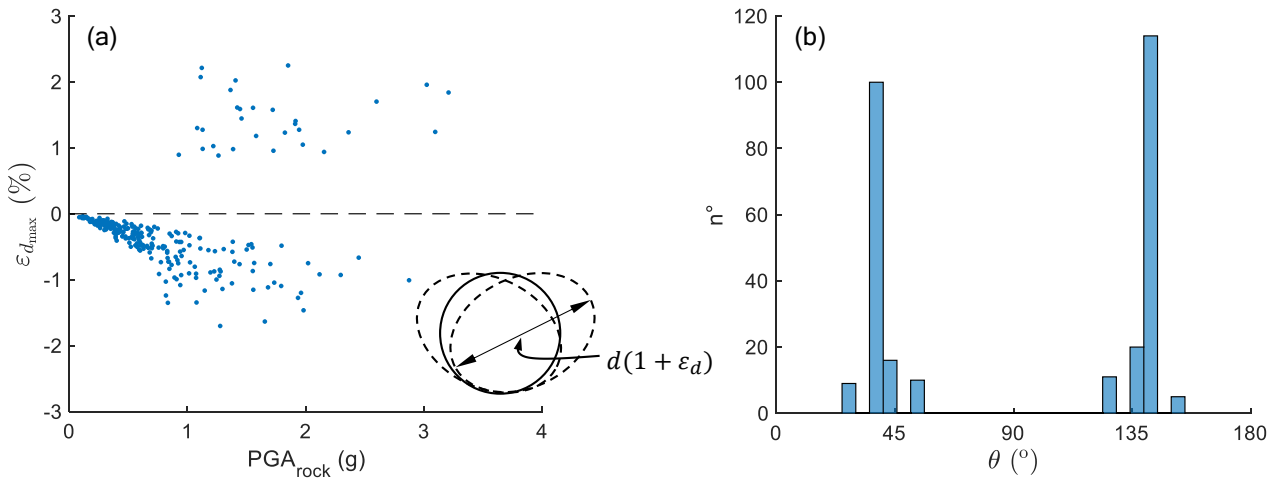


Fig. 9 – (a) Peak diametral strain versus input PGA, and (b) histogram of peak diametral strain location along the circumference

4.3 Seismic Risk Assessment

The annual rate of exceedance of tunnel EDPs was evaluated using two distinct methods. The first one, referred to as ‘risk by convolution’, follows PEER’s convolution of the seismic hazard curve and the EDP fragility function defined implicitly by Eq. (2). The second method, referred to as ‘scenario-based’ takes advantage of the rate of occurrence assigned to each ground motion as described above. Thus, analogous to Eq. (1), the rate of exceedance of an EDP takes the form of Eq. (3).

$$\lambda_{EDP} = \sum_{i=1}^{N_e} rate_i \cdot H(EDP - edp) \quad (3)$$



The annual rate of exceedance of the peak lining curvature, shear forces and axial loads is presented in Fig.10 using both formulations. For instance, the curvature associated to return periods of 500 and 1000 years is 0.0034 m^{-1} and 0.004 m^{-1} , respectively. The corresponding axial loads increments are $354 \text{ kN}\cdot\text{m}^{-1}$ and $386 \text{ kN}\cdot\text{m}^{-1}$. From this figure, it is apparent that the scenario-based risk curves match the convolution-based curves very well, in this case for exceedance rates less than 0.01 events/yr. Although the convolution approach produces continuous curves and seems to capture the entire range of exceedance rates, the fragility functions are not known a priori and, in general, their development is computationally intense.

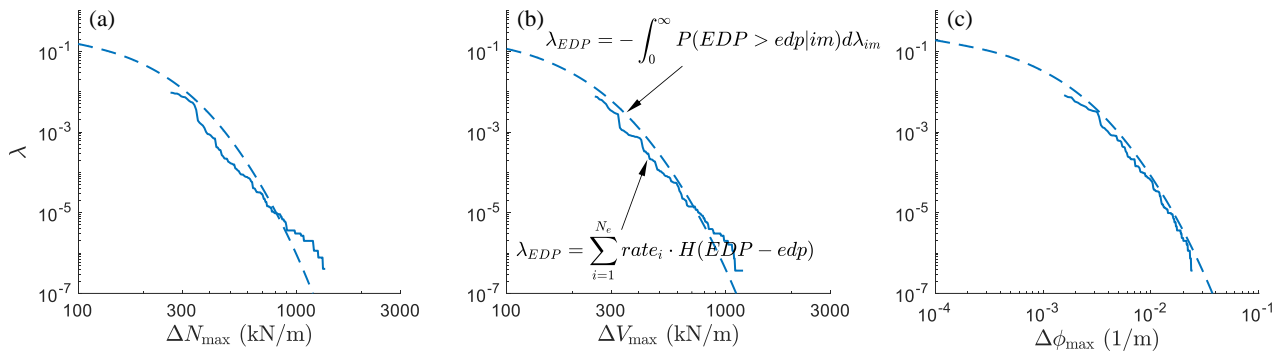


Fig. 10 – Risk curves for the dynamic increment of (a) axial load, (b) shear forces, and (c) lining curvature, obtained using the convolution (dashed lines) and scenario-based (continuous lines) approaches

Risk curves for other EDPs such as diametral strain, accelerations within the tunnel lining, or residual deformations can be derived with a similar approach, see more details in [25]. This allows quantifying the risk exposure of multiple tunnel components in a performance based framework and supports the risk informed decisions. Work is underway to extend the risk analysis of a single tunnel to evaluate risk in a tunnel network, where spatial variability of ground motions leads to spatial variability of damage.

5. Conclusions

This article presents fragility functions and quantifies risk on a tunnel through medium dense sand located on a shallow crustal setting. The results are derived from a plain strain finite element model that accounts for soil non-linearity and a simplified tunnel representation. A thorough validation of the soil parameters was performed in three levels; consisting of (1) single element tests, (2) shear waves propagation through a 1-D soil column, and (3) comparison of the seismic response of the soil-tunnel system against available centrifuge results. The seismic response of the model was evaluated for 285 records obtained from the PEER-NGA database, selected and scaled using a conditional scenario approach (CSS). From the study the following conclusions can be drawn:

- Validation of the soil constitutive relation at the element level is the most critical step in the model development. A correct characterization of stiffness and stress-strain cycles in single element tests was key to reproduce the centrifuge results.
- Both the centrifuge experiment and the plain strain numerical model are limited in their capacity to reproduce insitu K_0 conditions, which are rather an experimental outcome. In consequence, the dynamic response in both cases is expressed in terms of incremental variables with respect to the initial static conditions.
- The tunnel's bending moments increments (computed at the time of peak shear strains in the soil at the tunnel depth) are reasonably well approximated by Penzien's [8] solution derived from the theory of elasticity under the no-slip assumption.



- In flexible tunnels, i.e., coefficient of flexibility $F \gg 1$, the ovaling deformations are controlled by free field deformations, which can be used as a proxy to estimate the tunnel's seismic response and evaluate damage.
- The input PGA is an efficient parameter for the estimation of tunnel EDPs. In general, and despite the soil non-linearity, a linear relation was observed between $\log(\text{PGA})$ and $\log(\text{EDP})$, with residuals that follow a normal distribution.
- The scenario-based approach to compute seismic risk is an efficient method that does not rely on existing fragility functions. Its main advantage is the coherence between the local hazard, the use of region specific ground motions, and the causal relation between the ground motion intensities and tunnel response parameters.

6. Acknowledgements

This research was sponsored by FONDECYT Grant N°11180937 “Seismic Risk of Mined Tunnels”. Additional funding was provided by Facultad de Ingeniería Civil at Universidad del Desarrollo, FONDECYT Grant N° 1170836 “SIBER-RISK: SIMulation Based Earthquake Risk and Resilience of Interdependent Systems and NetworKs”, the Research Center for Integrated Disaster Risk Management (CIGIDEN) CONICYT/FONDAP/15110017. The authors are grateful for these supports.

7. Copyrights

17WCEE-IAEE 2020 reserves the copyright for the published proceedings. Authors will have the right to use content of the published paper in part or in full for their own work. Authors who use previously published data and illustrations must acknowledge the source in the figure captions.

8. References

- [1] Yang, Z., & Elgamal, A. (2003). Command Manual and User Reference for OpenSees Soil Models and Fully Coupled Element Developed at University of California at San Diego.
- [2] Bilotta, E., Lanzano, G., Madabhushi, G. S., & Silvestri, F. (2014). A numerical Round Robin on tunnels under seismic actions. *Acta Geotechnica*, 9(4), 563–579. <https://doi.org/10.1007/s11440-014-0330-3>
- [3] Power, M. S., Rosidi, D., & Kaneshiro, J. Y. (1998). Seismic vulnerability of tunnels and underground structures revisited. *Proceedings of the North American Tunneling*, 98, 243–250.
- [4] Yashiro, K., Kojima, Y., & Shimizu, M. (2007). Historical Earthquake Damage to Tunnels in Japan and Case Studies of Railway Tunnels in the 2004 Niigataken-Chuetsu Earthquake. *Quarterly Report of RTRI*, 48(3), 136–141. <https://doi.org/10.2219/rtriqr.48.136>
- [5] Yashinsky, M. (1998). *The Loma Prieta, California, Earthquake of October 17, 1989 - Highway Systems*. US Government Printing Office.
- [6] Kuesel, T. R. (1969). Earthquake Design Criteria for Subways. *Journal of the Structural Division*.
- [7] Wang, J. (1993). Seismic Design of Tunnels: A State-of-the-Art Approach. *William Barclay Parsons Fellowship*.
- [8] Penzien, J., & Wu, C. L. (1998). Stresses in linings of bored tunnels. *Earthquake Engineering and Structural Dynamics*, 27(3), 283–300. [https://doi.org/10.1002/\(SICI\)1096-9845\(199803\)27:3<283::AID-EQE732>3.0.CO;2-T](https://doi.org/10.1002/(SICI)1096-9845(199803)27:3<283::AID-EQE732>3.0.CO;2-T)
- [9] Atkinson, J. H., & Potts, D. M. (1977). Centrifugal model tests on shallow tunnels in sand. *Tunnels and Tunnelling*, 9(1), 59–64.
- [10] Tsinidis, G., Heron, C., Pitilakis, K., & Madabhushi, G. S. (2015). Centrifuge modelling of the dynamic behavior of square tunnels in sand. *Experimental Research in Earthquake Engineering*, 35(4), 509–523. <https://doi.org/10.1007/978-3-319-10136-1>



- [11] Yamada, T., Nagatani, H., Igarashi, H., & Takahashi, A. (2002). Centrifuge model tests on circular and rectangular tunnels subjected to large earthquake-induced deformation. In *Proceedings of the 3rd symposium on geotechnical aspects of underground construction in soft ground in Toulouse, France, 22-25 October*.
- [12] Lanzano, G., Bilotta, E., Russo, G., Silvestri, F., & Madabhushi, G. S. (2012). Centrifuge modeling of seismic loading on tunnels in sand. *Geotechnical Testing Journal*, 35(6), 854–869. <https://doi.org/10.1520/GTJ104348>
- [13] Andreotti, G., & Lai, C. G. (2015). Methodology to Derive Damage State-Dependent Fragility Curves of Underground Tunnels. In *66th International Conference on Earthquake Geotechnical Engineering (6ICEGE) in Christchurch, New Zealand, 2-4 November 2015*.
- [14] Argyroudis, S. A., & Ptilakis, K. D. (2012). Seismic fragility curves of shallow tunnels in alluvial deposits. *Soil Dynamics and Earthquake Engineering*, 35, 1–12. <https://doi.org/10.1016/j.soildyn.2011.11.004>
- [15] Visone, C., & Santucci de Magistris, F. (2009). Mechanical behaviour of the Leighton Buzzard Sand 100/170 under monotonic, cyclic and dynamic loading conditions. In *ANIDIS 2009 - XIII Convegno ANIDIS "L" ingegneria Sismica in Italia in Bologna, Italy, 28 Junio - 2 Julio*.
- [16] McKenna, F. (2011). OpenSees: a framework for earthquake engineering simulation. *Computing in Science & Engineering*, 13(4), 58–66.
- [17] Hardin, B. O., & Richart Jr, F. E. (1963). Elastic wave velocities in granular soils. *Journal of Soil Mechanics & Foundations Div*, 89.
- [18] Kuhlemeyer, R. L., & Lysmer, J. (1973). Finite element method accuracy for wave propagation problems. *Journal of Soil Mechanics & Foundations Div*.
- [19] Arteta, C. A., & Abrahamson, N. A. (2019). Conditional Scenario Spectra (CSS) for Hazard-Consistent Analysis of Engineering Systems. *Earthquake Spectra*, 35(2), 737–757. <https://doi.org/https://doi.org/10.1193/102116EQS176M>
- [20] Petersen, M. D., Moschetti, M. P., Powers, P., Mueller, C. S., Haller, K. M., Frankel, A. D., ... Olsen, A. H. (2015). The 2014 United States national seismic hazard model. *Earthquake Spectra*, 31(1), 1–30.
- [21] Seed, H. B., & Idriss, I. M. (1970). Soil moduli and damping factors for dynamic response analyses. *Earthquake Engineering Research Center, University of California Berkeley*.
- [22] Darendeli, M. B. (2001). Development of a new family of normalized moduli reduction and material damping curves.
- [23] Lanzano, G., Santucci de Magistris, F., & Bilotta, E. (2014). Calibration of the mechanical parameters for the numerical simulations of dynamic centrifuge experiments, 169–174.
- [24] Hashash, Y. M. A., Hook, J. J., Schmidt, B., & I-Chiang Yao, J. (2001). Seismic design and analysis of underground structures. *Tunnelling and Underground Space Technology*, 16(4), 247–293. [https://doi.org/10.1016/S0886-7798\(01\)00051-7](https://doi.org/10.1016/S0886-7798(01)00051-7)
- [25] Lyon, B. (2019). *Evaluación del Riesgo Sísmico de Túneles Circulares en Depósitos de Suelo* (Master's Thesis). Universidad del Desarrollo, Santiago, Chile.
- [26] Seed, R. B., Bray, J. D., Chang, S. W., & Dickenson, S. E. (1997). Site-dependent seismic response including recent strong motion data. In *14th International Conference on Soil and Foundation Engineering in Sitzungsberichte, Hamburg, Germany, 6 - 12 September* (pp. 125–134).
- [27] Anderson, D. G. (2008). Seismic Analysis and Design of Retaining Walls, Buried Structures, Slopes, and Embankments. *Transportation Research Board*. <https://doi.org/10.17226/14189>